



Article

The Hybrid Joints between an FRP Panel and a Steel Panel through Tubular Reinforcements: A Methodology for Interlaminar Stress Calculations

Franklin Domínguez ^{1,2,3,*}  and Luis Carral ⁴ 

¹ Doctoral Program, Universidade da Coruña, Campus Esteiro, 15403 Ferrol, Spain

² Chimborazo 2912 y Garcia Goyena, Guayaquil 090114, Ecuador

³ Escuela Superior Politécnica del Litoral, ESPOL, Facultad de Ingeniería Marítima y Ciencias del Mar - FIMCM, ESPOL Polytechnic University, Campus Gustavo Galindo Km. 30.5 Vía Perimetral, P.O. Box 09-01-5863, Guayaquil 090902, Ecuador

⁴ Department of Naval and Industrial Engineering, Universidade da Coruña, Campus Esteiro, 15403 Ferrol, Spain; lcarral@udc.es

* Correspondence: f.j.dominguez.ruiz@udc.es or jdominguez@tecnavin.com; Tel.: +59398-4166936

Received: 20 April 2020; Accepted: 2 June 2020; Published: 7 June 2020



Abstract: The advantages of laminates in terms of the chemical properties and mechanical properties/weight relationship have motivated several applications of fiber-reinforced plastic (FRP) composites in naval constructions due to the reduction in structural weight. This weight advantage has motivated multiple investigations dedicated to dissimilar material joints. We present a methodology for the interlaminar stress calculations of a tubular hybrid joint between an FRP panel and a steel panel through tubular reinforcements. The proposed formulas allow the estimation of the shear and normal stresses on the adhesive, which are generated in the bonding angle of the tubular hybrid joint. The stresses generated at the adhesive bonding ends influence on the adherent's adjacent layer. A failure criterion is shown to check the accomplishment of the resulting stresses in the adherent laminate. Finally, the proposed formulas are validated using the finite element method and compared with the obtained interlaminar stresses.

Keywords: hybrid joint; adhesive single-lap joint; interlaminar stress; tubular reinforcement joint; marine applications; composite

1. Introduction

The hybrid joint was developed from the technique of using adhesive and bolts to bond different materials, which are applied to join steel deck and fiber-reinforced plastic (FRP) panels. The different proposals of many researchers are summarized as follows: Ritter and Speth [1] developed a proposal for a hybrid union of a military ship, between a steel deck and composite superstructure with symmetrical connection is made using an adhesive double joint. This joint was proven by converting two German frigates into yachts. Rudiger and McGeorge [2] developed the symmetrical joint, an adhesive double type with a sandwich panel and without a bevel in connection. The joint was fixed using adhesive and supported by a mechanical fastening.

Hentinen and Hildebrand [3,4] developed an asymmetric single-type adhesive joint with a sandwich panel and transition bevel; the critical load of the joint was absorbed by the bolts. Bohlmann and Fogarty [5] proposed a hybrid joint with bolts, adhesive, and a steel plate that could be welded directly to the deck and screwed or joined to a sandwich-type laminate. Kotsidis, Kouloukouras, and Tsouvalis [6] analyzed the finite elements of a sandwich-type joint, but with a modification, including the inner end of a folded steel plate. Shkolnikov [7] proposed a hybrid joint between steel

panels and FRP panels; this union has been called 'Comeld-2'. This study focused on the application of composite panels in military and submarine ships. Simler and Brown [8] proposed a US Navy ONR's Navy Joining Center (NJC) adhesive joint consisting of a metal *H* profile to generate an adhesive double joint, which is to be welded to the deck. The lamination used was vinyl ester resin and a balsa core.

Boyd, Blake, Sheno, and Kapadia [9] performed a local fatigue analysis on a composite-steel panel, between the joint of the deck and the side of a frigate superstructure. Ozes and Nesar [10] conducted experimental tests of hybrid joints between steel and fiber-reinforced panels, using the infusion method, for different roughness states of the steel. Babazadeh and Khedmati [11], in their publication, analyzed the effect of the main parameters of the hybrid joint, sandwich-type with adhesive, through applying tension loads. Johansson [12] and Beeston [13] studied the type of construction used by the Kockums shipyard for the joints of reinforced fiberglass/carbon fiber reinforced polymer (CFRP) superstructures with steel hulls. The panel contact was made on the U profile through adhesives.

The mentioned hybrid joints were applied mainly to join FRP superstructures, masts, and accessories to a metal structure. The proposed joints were mostly of the adhesive type, and a few involved fixing bolts. The methods proposed had some limitations as follows: the difference between the thermal expansion coefficients; the corrosive effect if the steel structure was used; the difficulty of fixing the FRP panel girders to the metal structure; and the fixing of the interface structure to the metal panel. In the present investigation, we used a tubular hybrid joint, as proposed in [14,15], as an option that allowed the following: prefabricating the FRP block, minimizing the difference in the thermal expansion coefficients, and minimizing the corrosive effect due to the metal surfaces that are protected with an adequate epoxy anticorrosive treatment.

Researchers proposed different techniques for the analytical study of adhesive single-lap joints; these methods can be classified as explicit and implicit. Explicit methods to estimate shear and normal stresses (closed form) are as follows: Volkersen [16] was the first to study single adhesive joints, he only proposes the shear stress formula because it does not consider deformations in the adherents. Goland and Reissner [17] propose formulas considering the deformation in the adherents due to the bending moment generated by the eccentricity of the applied force, its method only applies to balanced joints and thin adherents. Hart-Smith [18–22] developed formulas for the stresses considering elastic and plastic adhesive material for balanced and unbalanced joints. Allman [23] developed the formulas for balanced joints considering a non-deformable geometry, concluding that the shear stresses do not vary along with the adhesive. Bigwood and Crocombe [24,25] investigate the shear and normal stresses applicable to various adhesive joint configurations and different adherents, with simplified formulas that are easy to apply. Oplinger [26] following the work of Goland and Reissner, modified the formulas to estimate the stress of the adhesive, considering the thickness of the adhesive and different thicknesses of the adherents. Zou [27] proposed easy-to-apply formulas for estimating adhesive joints only for balanced adherents. These explicit methods are applied for adherents and adhesives with isotropic properties and linear-elastic analysis.

Implicit methods include the following: Renton and Vinson [28] who developed an ordinary linear differential equation of the eighth order, where they consider anisotropic adherents and isotropic adhesive. Ojalvo [29], based on the Goland and Reissner method, analyzed the influence of the thickness of the adhesive on the adhesive joint. Adam and Mallick [30] included the influence of thermal loads on the adhesive bond and the modelling of the spring-loaded adhesive and presented formulas for the stresses on the top and bottom of the adhesive. Smeltzer [31] proposed formulas considering elastic anisotropic adherents and elastic-plastic isotropic adhesive. These methods recommend using numerical methods and/or finite elements depending on the case to complete the estimation of the stresses of the adhesive joints.

The mentioned methods have proposed formulas to statically estimate the stresses and their distribution in the adhesive, however, they have not taken into consideration the behavior of the joint subjected to vibratory loads. These studies are presented by Det Norske Veritas (DNV) [32],

Hollaway [33], and Huang et al. [34], allowing them to estimate the S–N curve of the joint based on the operating cycles.

In this investigation, the methodology consists of using general formulas to calculate the stresses of adhesive joints applied in a tubular hybrid joint (see Figure 1), and the accomplishment of a failure criterion of interlaminar stresses in the laminates of the adherents. From the different tests performed with finite element analysis (FEA), it was proved that the tubular reinforcement laminate behaves like an adhesive single-lap joint. Bigwood and Crocombe [24] formulas are used due to different thicknesses and stiffness of the adherents of this joint. These formulas have been validated by Nhamoinesu and Overend [35] and Riccio and Sellitto [36] using FEA. Nhamoinesu [35] applied the method to select the epoxy and acrylate adhesive based on the mechanical performance of the bond and subjected to short-duration loads; this analytical method has shown good results with small deformations in the adhesive (30% of the maximum deformation). However, it loses accuracy with greater deformation compared with the nonlinear FEA results. Riccio [36] apply the Bigwood [24] method as it is of general use in adhesive joints; they used an L-shaped symmetric T-pull model modelled in FEA with four nodes 2D plane elements, finding satisfactory results in the extreme stress values and the distribution along with the adhesive.

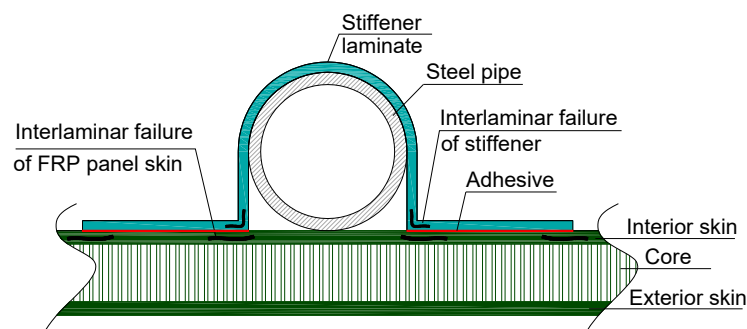


Figure 1. Schematic indicating the typical interlaminar failures in a hybrid joint with tubular reinforcement.

From the results of the different studies, we found that depending on the characteristics of the adhesive joint, the adhesive or the interface between the FRP laminates adherents 1 and 2 may fail [18]. For this reason, when studying a hybrid joint using tubular stiffeners, consideration should be given to the following:

1. The limit of the interlaminar stresses of the adherents, Hou [37].
2. The fatigue on the joint to guarantee its useful life, DNV [32].

For the study of interlaminar stress, the following tubular hybrid joint configuration is considered:

- Adherent 1: fiberglass laminated over the metal pipe.
- Adherent 2: a sandwich panel FRP.
- Adhesive: a 250-micron polyester resin layer.

The orthotropic properties for adherent laminates 1 and 2, are in Appendix A: (Tables A1–A3); the formulas to calculate the 3D stress-strain matrix, the transversal properties of the individual ply, the equivalent isotropic properties, are in Appendix B.

2. Methodology

The proposed methodology is used to obtain the resulting stresses at the ends of the adhesive based on the equivalent isotropic properties of adherents 1 and 2. The simplified formulas proposed by Bigwood/Crocombe [24] to calculate the stresses in the adhesive has the limitation that does not consider the coupling between normal and shear stresses, due to this limitation, the results are useful

for a preliminary analysis of the tubular hybrid joint. Second, the interlaminar stress analysis in the adherent's adjacent outer layer is carried out, because the properties of the individual ply of the adjacent layers are considered. This part is a localized microstructural analysis to study laminate debonding as a result of fatigue, this debonding is avoided when the quadratic-type failure criterion is met.

2.1. Proposed Formulas for Tubular Hybrid Joint

In this section, a mathematical model concerning the behavior of tubular reinforcement on an FRP panel is formulated. For the analysis, we considered that the reinforcement in the panel remains attached by the adhesive.

2.1.1. Macro-Structural and Microstructural Analysis

The macro-structural analysis consisted of considering the composite laminate as a monolithic-type solid-elastic body, and allowed a preliminary estimation, based on the following considerations, [38]:

- The structural laminate has a linear behavior; therefore, it complies with Hook's Law [18].
- Transversal deformations due to shear stress are negligible.
- Deformations vary linearly across the thickness.
- The unitary elongation in the vertical direction is considered as being negligible compared to the unitary elongations of the horizontal plane.
- The laminate is quasi-isotropic.
- The formulas for macro-structural analysis are based on the classical theory of plates. The structural laminate panel is considered as being circumscribed and fixed between girders.

The microstructural analysis considered that the layers of the laminate can be approximated with a rectangular laminate stack. This allowed the final estimation of the stresses and deformations of each laminate layer. This type of analysis is also known as a 'critical layer' study.

2.1.2. Adhesive Model Considerations

The normal and shear stresses of the adhesive model had the following considerations:

- The Bigwood/Crocombe [24] model considers the adhesive as isotropic, elastic, and linear;
- The adherent's properties are considered isotropic and can be of different thicknesses;
- The adhesive used is polyester resin with the same characteristics of those considered in the Bigwood/Crocombe model [24];
- The adhesive joint of the panel tubular reinforcement is analyzed according to the theory of elasticity;
- A typical diagram of the joint between the reinforcement and the panel is shown in Figure 2;
- The distance L of the joint length;
- The equations of motion are obtained assuming that the panel has a cylindrical flexure behavior.

Equations of Motion in Terms of Normal and Shear Stress, Simplified Analysis

For normal stress, the equation of motion is simplified, based on the consideration that the variation of the shear stress along the joint is lesser in importance [24].

$$\frac{d^4 \sigma_z}{dy^4} + 4K_5^4 \sigma_z = 0, \quad (1)$$

where:

$$K_5^4 = \frac{E_a}{4 \cdot t} \left(\frac{1}{D_1} + \frac{1}{D_2} \right), \quad (2)$$

using the following compliance factors for the normal stress calculation:

$$\beta_1 = \frac{12 \cdot E_a \cdot (1 - \mu_1^2)}{E_1 \cdot h_1^3 \cdot t}, \tag{3}$$

$$\beta_2 = \frac{12 \cdot E_a \cdot (1 - \mu_2^2)}{E_2 \cdot h_2^3 \cdot t}. \tag{4}$$

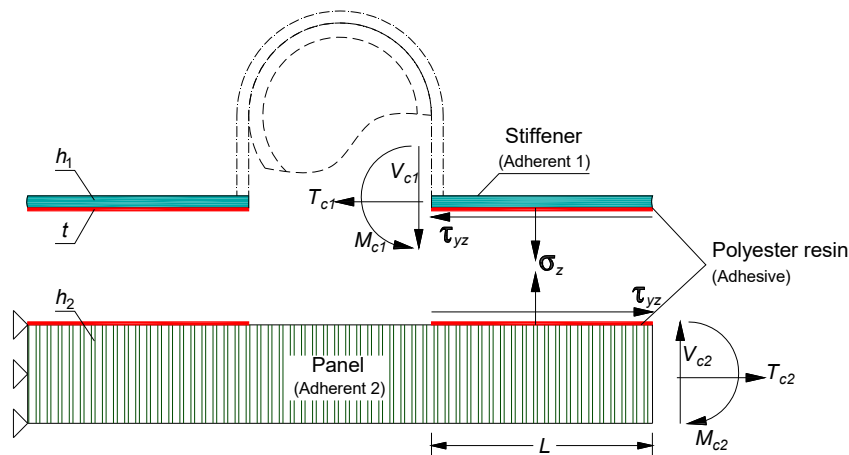


Figure 2. Typical diagram of the stiffener-panel joint.

Based on compliance of these two factors (Equations (3) and (4)), the following formulas are obtained to determine the maximum values of normal stresses:

$$\sigma_{V_c} = \frac{-(2)^{0.5} \cdot \beta_1 \cdot V_c}{(\beta_1 + \beta_2)^{0.75}}, \tag{5}$$

$$\sigma_{M_c} = \frac{-\beta_1 \cdot M_c}{(\beta_1 + \beta_2)^{0.5}}. \tag{6}$$

For the shear stress, the following motion equation is simplified, based on the assumption that the variation of the normal stress along the joint is small.

$$\frac{d^3 \tau_{yz}}{dy^3} - K_6^2 \frac{d\tau_{yz}}{dy} = 0, \tag{7}$$

where:

$$K_6^2 = \frac{4 \cdot G_a}{t} \left(\frac{(1 - \mu_1^2)}{E_1 \cdot h_1} + \frac{(1 - \mu_2^2)}{E_2 \cdot h_2} \right), \tag{8}$$

using the following compliance factors for the calculation of shear stress:

$$\alpha_1 = \frac{G_a \cdot (1 - \mu_1^2)}{E_1 \cdot h_1 \cdot t}, \tag{9}$$

$$\alpha_2 = \frac{G_a \cdot (1 - \mu_2^2)}{E_2 \cdot h_2 \cdot t}. \tag{10}$$

Based on the compliance of these two factors (Equations (9) and (10)), the following formulas are obtained to determine the maximum values of shear stresses:

$$\tau_{T_c} = \frac{-\alpha_1 \cdot T_c}{2 \cdot (\alpha_1 + \alpha_2)^{0.5}}, \tag{11}$$

$$\tau_{V_c} = \frac{3 \cdot V_c}{4 \cdot h_1}, \tag{12}$$

$$\tau_{M_c} = \frac{3 \cdot \alpha_1 \cdot M_c}{h_1 \cdot (\alpha_1 + \alpha_2)^{0.5}}. \tag{13}$$

The definition of the variables V_c , T_c , and M_c are indicated in Figure 2.

These formulas can be applied to two types of panels the single laminate and the sandwich laminate. Following the model considerations indicated in Section 2.1.2, we expected to estimate the stress to occur in the adhesive.

2.2. Forces and Moments on the Tubular Hybrid Joint

The elastic model of Bigwood/Crocombe [24] satisfied the model considerations proposed in Section 2.1.2 and allows us to estimate the adhesive stress of the tubular hybrid joint. To apply these simplified formulas in the tubular hybrid joint, it is necessary to define the forces and moments, as explained below.

In Figure 3, we considered that the reinforcement is subjected to forces (P , V , T) in three directions. In this study, the forces used in the formulas proposed by Bigwood/Crocombe [24] are applied per unit length (see Section 2.1.2 and Appendix C).

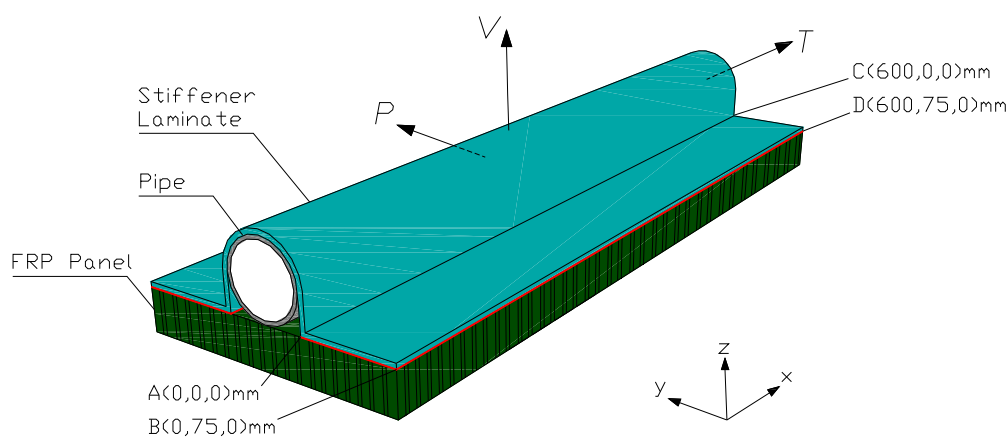


Figure 3. Applied forces on the hybrid joint panel and stiffener.

Where:

- P is the force in the y -direction on the hybrid reinforcement; this force generates an equivalent moment M' exerted in the tubular laminate. This moment is estimated as follows (see Figure 4):

$$M' = \frac{M}{6} = \frac{P \cdot D}{12}. \tag{14}$$

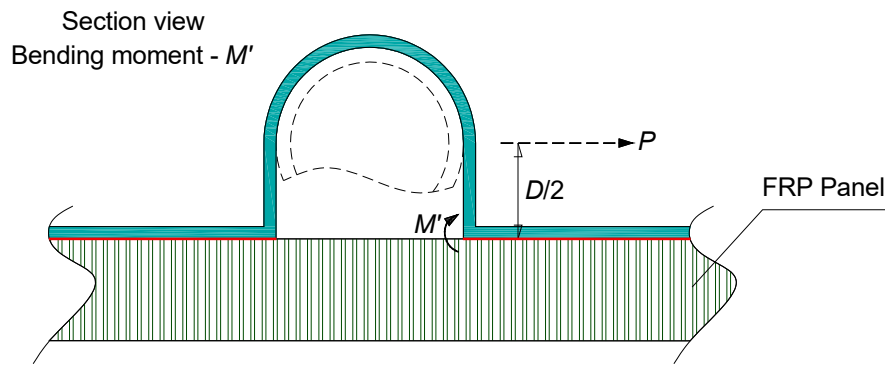


Figure 4. The equivalent moment on the hybrid panel and stiffener.

- V is the force on the hybrid reinforcement in the z -direction. This force is broken into its two components (V_z, V_y), separated by the pipe diameter D . See Figure 5a, on both sides of the tubular laminate. The components are defined as follows:

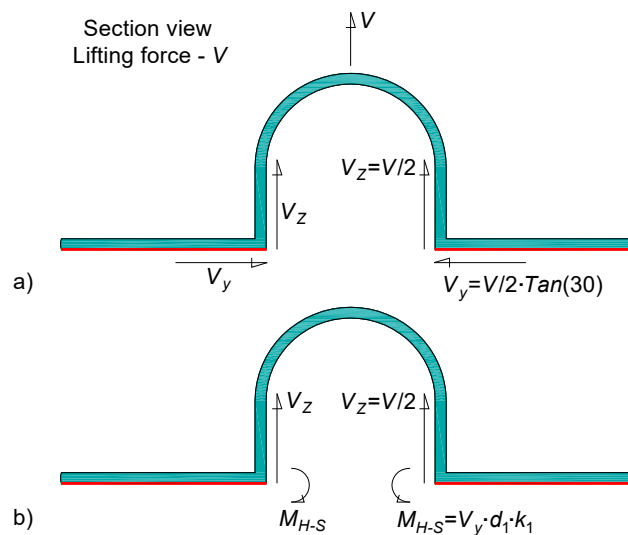


Figure 5. Equivalent lifting forces: (a) vertical force V decomposition, (b) lifting forces, and moment on the stiffener laminate.

$$V_z = \frac{V}{2}, \quad V_y = \frac{V}{2} \cdot \tan(30). \quad (15)$$

The component (V_y) generates a moment in Adherent 1. The behavior of the tubular laminate in the y -direction is similar to that proposed by Hart-Smith's moment equation [18], see Figure 5b:

$$M_{H-S} = V_y \cdot d_1 \cdot k_1, \quad (16)$$

in which:

$$k_1 = \frac{1}{1 + \xi_1 \cdot c + \frac{(\xi_1 \cdot c)^2}{6}}, \quad (16a)$$

$$\xi_1^2 = \frac{12 \cdot V_y \cdot (1 - \mu_1^2)}{k_b \cdot E_1 \cdot h_1^3}. \quad (16b)$$

- T is the force applied to the tubular laminate in the x -direction; this force is applied to both the laminates and the root to obtain the adhesive shear stress.

Application to Tubular Hybrid Joint

A typical application of the hybrid tubular joint between a steel deck and FRP panel of a superstructure is presented in Figure 6. The proposed methodology allows estimating the adhesive stresses, so it is necessary to define the forces (P, V, T), these forces must be calculated in advance to be applied over a tubular hybrid joint of the FRP panel, under pressure p (kN/m²).

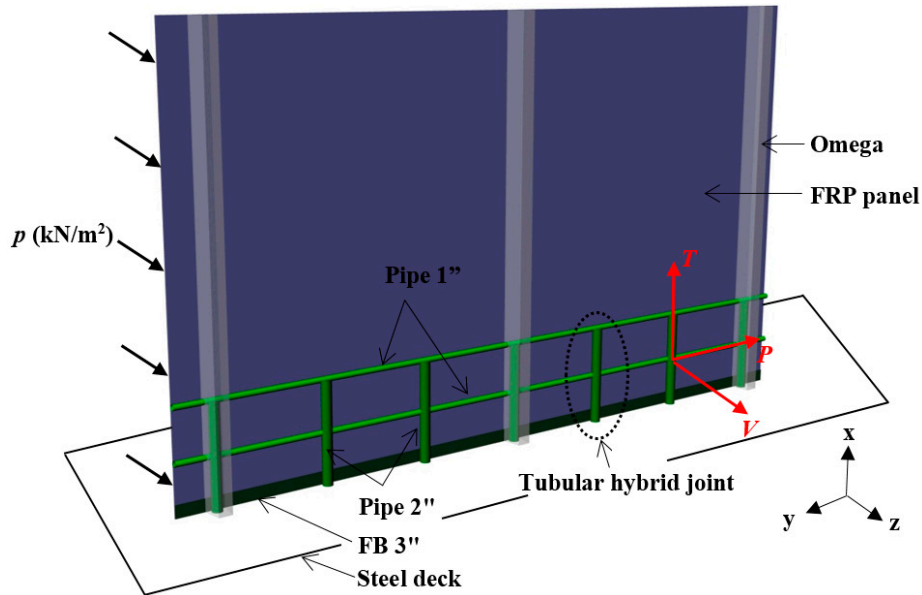


Figure 6. Typical assembly of tubular hybrid joint.

To estimate the resultant forces (P, V, T) on the pipes of the hybrid joint, a global analysis of a superstructure subjected to a pressure p is performed, additionally considering a heeling or pitching. The magnitude of p and the heel or pitch is recommended by the classification society.

In cases where the hybrid joint is installed on the steel deck where there is auxiliary equipment, the moments transferred from the deck to the panel should be added in calculations.

2.3. Interlaminar Stresses

2.3.1. Failure Criteria

Once the shear and normal adhesive stresses resulting from the applied forces are obtained with equivalent isotropic properties, it is important to evaluate the combination of the interlaminar stresses of the adherent's adjacent outer layer with the properties of the individual ply. The stresses resulting from the Bigwood/Crocombe [24] formulas are considered decoupled by definition. Therefore, the quadratic criterion of Tsai-Hou [37], Equation (17), is selected as the failure criterion.

$$\sigma_z \geq 0, \quad \left(\frac{\sigma_z}{Z_t}\right)^2 + \left(\frac{\tau_{xz}^2 + \tau_{yz}^2}{S_t^2}\right) \geq 1. \tag{17}$$

When designing a panel with stiffeners, the type of load to be applied or the fatigue to which it is being subjected must be considered. For this reason, when evaluating the quadratic failure criterion (Equation (17)), the calculated static stresses must be reconsidered as virtual stresses, which includes the type of load to which they are being subjected. These virtual stresses are defined as follows [33]:

$$\sigma_z' = \frac{\sigma_z}{F_{rc-i}'} \tag{18a}$$

$$\tau_{xz}' = \frac{\tau_{xz}}{F_{rc-i}}, \tag{18b}$$

$$\tau_{yz}' = \frac{\tau_{yz}}{F_{rc-i}}. \tag{18c}$$

The modified failure criterion is proposed considering the virtual stresses as indicated:

$$\sigma_z \geq 0, \quad \left(\frac{\sigma_z'}{Z_t} \right)^2 + \left(\frac{(\tau_{xz}')^2 + (\tau_{yz}')^2}{S_t^2} \right) \geq 1 \tag{19a}$$

where:

$$\sigma_z \geq 0, \quad \left(\frac{\sigma_z}{F_{rc-i} \cdot Z_t} \right)^2 + \left(\frac{(\tau_{xz})^2 + (\tau_{yz})^2}{F_{rc-i}^2 \cdot S_t^2} \right) \geq 1. \tag{19b}$$

According to Equations (5), (6), and (11)–(13) applied to the tubular hybrid joint, we considered the following:

$$\sigma_z = \sigma_{M_c-P} + \sigma_{V_c-V_z}, \tag{20a}$$

$$\tau_{xz} = \tau_{T_c-T}, \tag{20b}$$

$$\tau_{yz} = \tau_{M_c-P} + \tau_{V_c-V_y}. \tag{20c}$$

The formulas indicated are based on linear theory; therefore, the principle of stress superposition can be applied when the resulting stresses are in the same direction. To carry out the optimization process, we considered that not only the first layer must comply with the failure criteria, but all the layers of the laminate including the core must also comply if this is applicable. For this, a matrix must be generated to estimate the behavior of each laminate layer. To estimate the stresses in the successive layers, the formulas proposed by Special Service Craft (SSC) Lloyd’s Register [39] can be used to verify that the failure criterion is met.

2.3.2. Limit Interlaminar Stresses

The normal and shear stresses’ limits in an interlaminar depend on the amount of fiber and the type of resin used. Table 1 shows the limit values of the interlaminar stresses for a laminate with an orthophthalic polyester resin. In the case where one of these parameters is not available, it can be estimated using the following dimensionless relationship (Equation (21b)).

$$\frac{Z_{t_1}}{S_{t_1}} \cdot \left(\frac{E_{m1}}{E_{i1}} \right)^{1/2} = \frac{Z_{t_2}}{S_{t_2}} \cdot \left(\frac{E_{m2}}{E_{i2}} \right)^{1/2} \tag{21a}$$

$$Z_{t_2} = Z_{t_1} \cdot \frac{S_{t_2}}{S_{t_1}} \cdot \left(\frac{E_{m1}}{E_{m2}} \right)^{1/2} \cdot \left(\frac{E_{i2}}{E_{i1}} \right)^{1/2} \tag{21b}$$

Table 1. Estimation of the failure stresses in the interlaminar.

Fiber	f _c ⁽¹⁾	S _t ⁽¹⁾	Z _t
		(MPa)	(MPa)
Uni-directional (UD)	60%	15.00	14.60 ⁽¹⁾
Woven Roving (WR)	50%	15.25	11.70 ⁽³⁾
Chopped strand mat (CSM)	30%	17.95	9.50 ⁽³⁾

(1) Lloyd’s Register [39], (3) Z_t estimated using Equation (21b). Note: see laminate properties (E_{mj} y E_{ij}), in Appendix A.

For cases in which the FRP panel is of sandwich-type, with a balsa core, additional consideration must be given to the tensile, compression, and shear stresses of the core, see Lloyd's Register [39]: Table 2.2.2 Minimum characteristics and mechanical properties of end-grain balsa.

2.3.3. Design Factors: Interlaminar Stress Fraction

When designing an adhesive hybrid joint, the type of force that the panel is subjected to must be considered to estimate the life of the hybrid joint. Hollaway [33] recommended using the fractions of interlaminated stress for the design of a hybrid joint, depending on the life cycle, see Hollaway [33]: Table 5.2 Typical long term load reduction factors for GFRP: data refer to the ratio of long term strength/short term strength at ambient test conditions.

As a reference, Lloyd's Register [39] recommended using the failure stress fraction for tension or compression stresses [0.3–0.4], and shear stresses [0.33], according to the application area.

3. Results: Single-Lap Joint Validation by Applying FEA

The model of a cruising yacht, 36.80 m, proposed in [14] is used for this validation, which consists of applying a design pressure of 5.16 kN/m² on the side of the first port side deck with an area of 48.78 m² and a heeling of 30° to starboard, without considering any moment transmitted from the deck. Resultant forces on an intermediate tubular connection between the omegas are (see Figure 6) $P = 134$ [N], $V = 5127$ [N], $y T = 4899$ [N].

Figure 3 shows the model used for the validation of a tubular hybrid joint, which consists of a 600 × 210 × 32.9 mm FRP panel, a 2" Sch40 steel pipe, and a tubular laminate with four layers of fiberglass over the pipe, the laminate sequence stacking and properties are in Table A2. To apply the formulas in Section 2.1.2 and Appendix C, the equivalent isotropic properties must be estimated from the orthotropic properties (see Appendix B).

3.1. Numerical Model

For comparison of results, finite element analysis is performed; 2D and 3D models are developed using Ansys software, considering the orthotropic properties of the laminate in each adherent. A 0.1 mm polyester resin interface layer is modelled between each layer of the laminates. The 3D model is analyzed with the ACP-Ansys module since it allows entering the properties of the adherents per layer; the adherents are modelled using shell elements and the adhesive using solid elements.

For the 2D model, only the Static Structural module with plain strain configuration is used since it allows analyzing the behavior of laminates and interfaces in the tubular hybrid joint. Software tools for mesh quality analysis are used and the convergence of the stress results with the indicated mesh for the 2D and 3D models, is achieved using a mesh refinement as indicated below:

- **Software:** Ansys Academic;
 - Module: ACP Pre, ACP Post and Static Structural;
- **Meshing 3D:** Model size 600 mm, general mesh 4 mm, refinement to 1.5 mm on a 30 mm radius on pipe corners, and to 0.2 mm on the middle panel on a 10 mm radius. The adhesive has three elements through-thickness, (see Figure 7a);
 - Nodes: 69,367;
 - Element: Quadrilateral Dominant;
- **Meshing 2D:** Model size 210 mm, general mesh 0.7 mm and refinement to 0.15 mm on a 6 mm radius on adhesive ends. The adhesive has two elements through-thickness, (see Figure 7b);
 - Nodes: 99,482;
 - Element: Quadrilateral Dominant.

- **Modeling:** The metal pipe is not considered in the validation.
- **Boundary conditions:** The panel is considered as being simply supported in the (x, y, z) directions, at the ends of the panel (adherent 2). The tubular laminate (adherent 1) is considered as being free at its ends.
- Forces:
 - For the x -direction (T):
 - The force is applied, taking into consideration the entire laminate surface of the reinforcement excluding the bonding tubular laminate over the panel.
 - For the y -direction (P):
 - The force is applied on the side of the tubular laminate at a remote point in the center of the metal pipe.
 - For the z -direction (V):
 - The force is applied, taking into consideration the entire laminate surface of the reinforcement excluding the bonding tubular laminate over the panel.

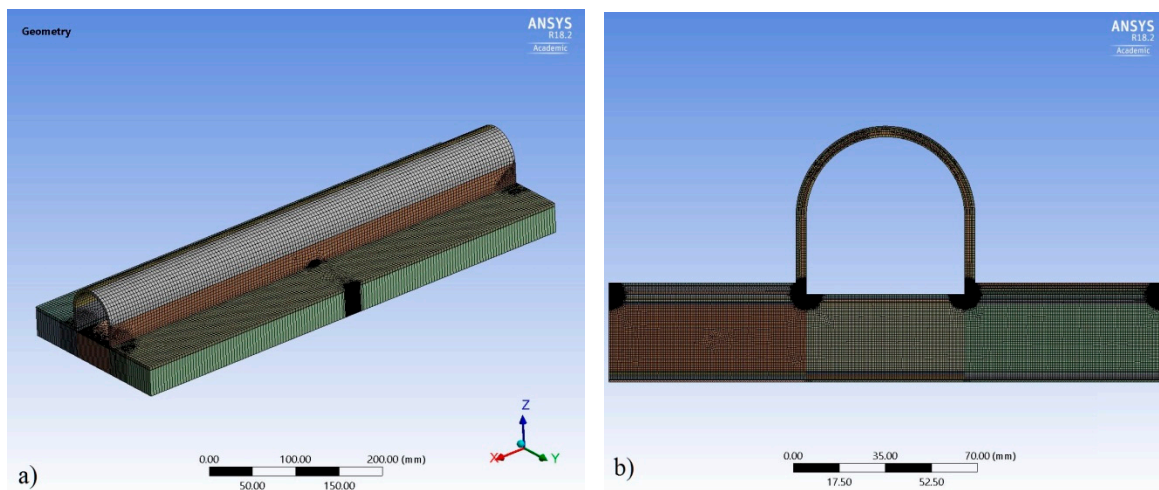


Figure 7. (a) 3D model: fiber-reinforced plastic (FRP) panel 210×600 mm, with 2" pipe laminate, (b) 2D model: FRP Panel 210 mm by unitary width, with 2" pipe laminate.

3.2. Results

The following Figures 8–10 present the comparison of stresses obtained from 2D, 3D FEA models and the general formulas of Bigwood and Crocombe [24] presented in Appendix C. The stress curves of formulas [24] show similar behaviors to the results obtained with the numerical analysis (FEA), however, the normal stress generated by the T force (Figure 8a) is zero.

The distribution of the maximum shear stresses of the T force, from the 3D model, at the first interface stress distribution between layers 1 and 2 of adherent 1 is presented in Figure 11.

The distribution of normal and shear stresses on adhesive and adherent 1 interfaces resulting from the V force, 2D model, are presented in Figure 12.

The results obtained in the adhesive at the endpoints A and B (Figure 3) with the proposed normal and shear stress formulas, and stresses calculate with FEA are presented in Tables 2 and 3 corresponding to the forces P , V , and T . Only results are presented in points A and B because they have greater values than points C and D. These tables present the application of the failure criterion (Equation (19b)), showing that the criterion is met.

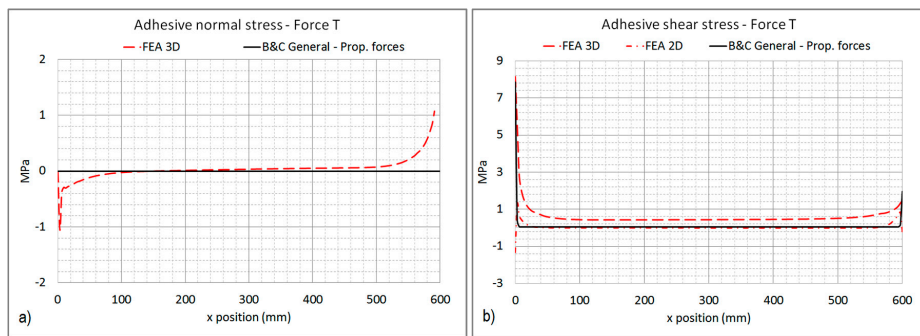


Figure 8. Force *T*, *x*-direction: stress curve, (a) normal, (b) shear.

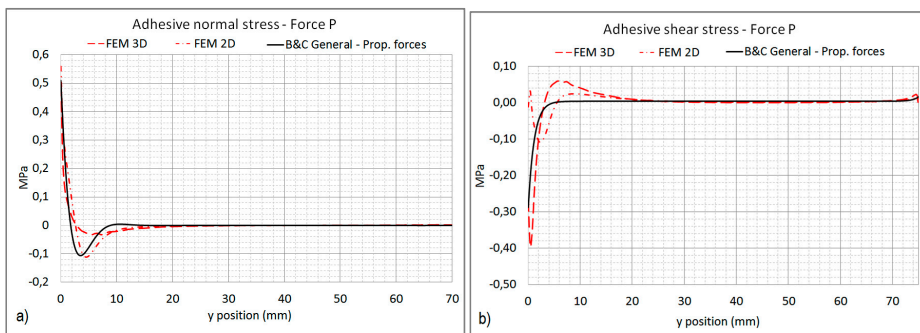


Figure 9. Force *P*, *y*-direction: stress curve, (a) normal, (b) shear.

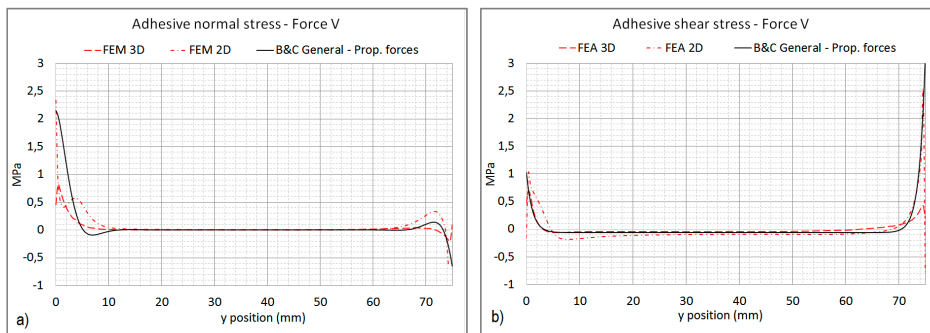


Figure 10. Force *V*, *z*-direction: stress curve, (a) normal, (b) shear.

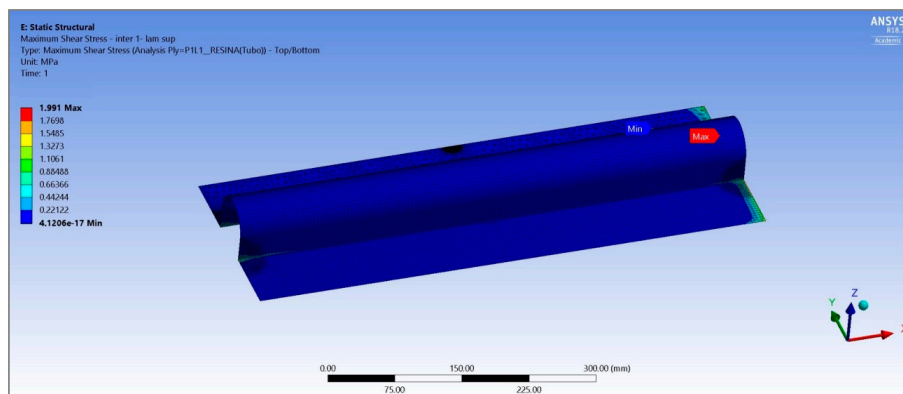


Figure 11. Force *T*, *x*-direction, from the 3D model: first interface stress distribution between layers 1 and 2 of adherent 1.

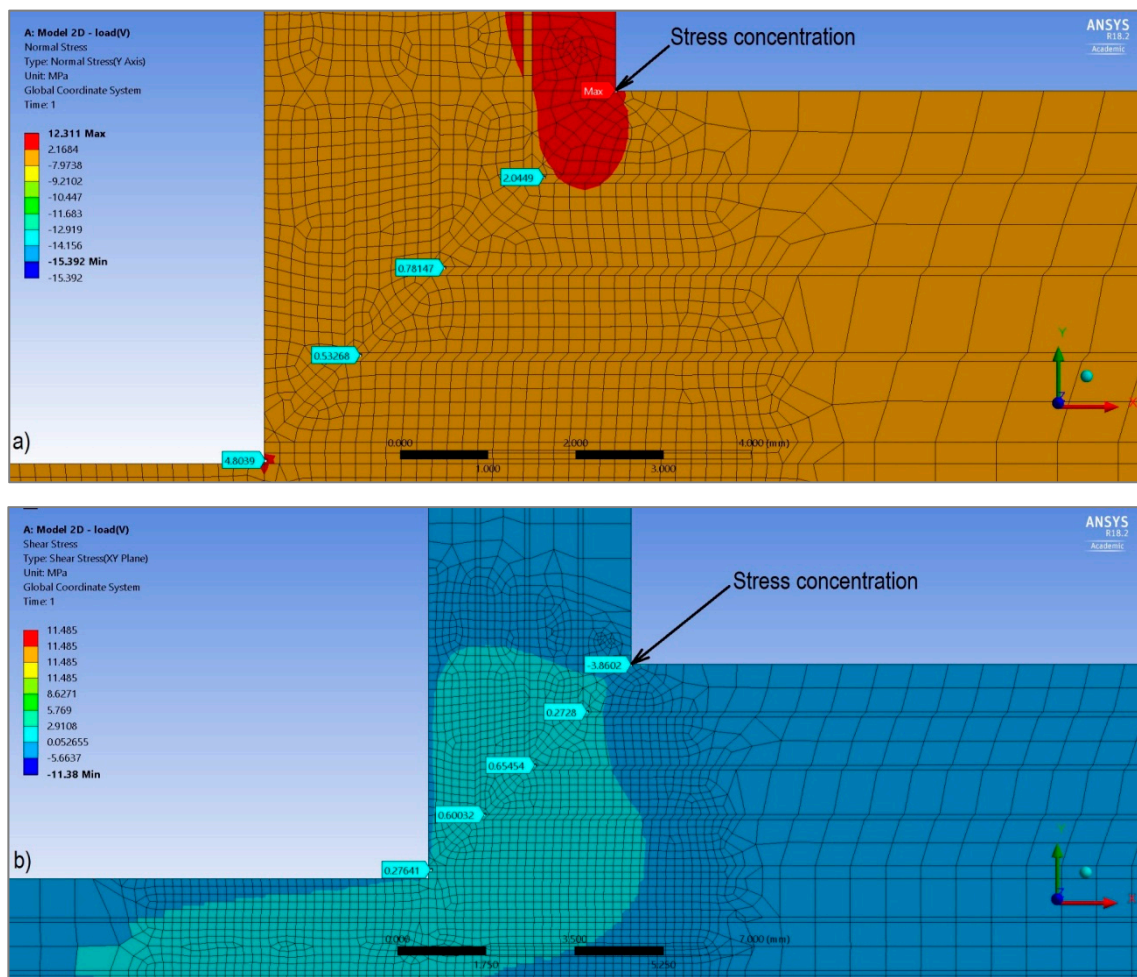


Figure 12. Force V, z-direction, from the 2D model: stress distribution, (a) normal, (b) shear.

Table 2. Failure criteria the tubular hybrid joint: Bigwood and Crocombe formulas.

Variable	Value	Bigwood and Crocombe Formulas					
		A (0,0,0) mm			B (0,75,0) mm		
		σ (MPa)	τ (MPa)		σ (MPa)	τ (MPa)	
		z	yz	xz	z	yz	xz
T (N/mm)	4899	0.000	-	7.858	0.000	-	7.858
V (N/mm)	5127	2.148	1.031	-	-0.652	3.076	-
P (N/mm)	134	0.509	-0.287	-	-0.003	0.016	-
σ_z (MPa)		2.657	-	-	-0.655	-	-
τ_{yz} (MPa)		-	0.744	-	-	3.092	-
τ_{xz} (MPa)		-	-	7.858	-	-	7.858
Z_t (MPa)			9.500			9.500	
S_t (MPa)			17.950			17.950	
Interlaminar Stress Fraction, F_{rc-i}			0.650			0.650	
Failure Criteria			0.500			0.510	

Table 3. Failure criteria the tubular hybrid joint: FEA.

Variable	Value	FEA					
		A (0,0,0) mm			B (0,75,0) mm		
		σ (MPa)	τ (MPa)		σ (MPa)	τ (MPa)	
		z	yz	xz	z	yz	xz
T (N/mm)	4899	-0.006	-	8.152	-0.006	-	8.152
V (N/mm)	5127	2.330	1.020	-	-0.610	2.480	-
P (N/mm)	134	0.493	-0.393	-	-0.014	0.023	-
σ_z (MPa)		2.817	-	-	-0.629	-	-
τ_{yz} (MPa)		-	0.627	-	-	2.503	-
τ_{xz} (MPa)		-	-	8.152	-	-	8.152
Z_t (MPa)			9.500			9.500	
S_t (MPa)			17.950			17.950	
Interlaminar Stress Fraction, F_{rc-i}			0.650			0.650	
Failure Criteria			0.540			0.520	

Using the formulas of the failure criterion it is possible to obtain the limit values of the safety factor S_f and the design pressure p that the adhesive joint can withstand. Table 4 presents the limit design pressure p , keeping constant interlaminar stress fraction at 0.650. Similarly, Table 5 presents as an alternative to the maximum safety factor S_f to which this FRP panel can be subjected, maintaining a constant design pressure of 5.160 kN/m². These indicated limit values of p and S_f application are subject to compliance of the critical layer analysis of FRP panel proposed by SSC-Lloyd’s Register, [39].

Table 4. Design limit pressure using the failure criteria.

	Pressure Factor	Design Pressure, p (kN/m ²)	Failure Criterion
p (initial)	1.000	5.160	0.540
p (maximum)	1.360	7.030	1.000

Table 5. Safety factor using the failure criteria.

	Safety Factor	Failure Criterion
F_{rc-i} (initial)	1.540	0.540
F_{rc-i} (minimum)	2.080	1.000

The safety factor S_f is defined as:

$$S_f = \frac{1}{F_{rc-i}} \tag{22}$$

4. Discussion

The method proposed by Bigwood and Crocombe includes simplified and general formulas that allow knowing the maximum and distributed values of the normal and shear stresses along with the adhesive. The results obtained with both formulations result in similar values and simplified formulas allow the quick estimation and easy application.

2D and 3D models have the same boundary conditions, making it possible to make a comparison between the results of the stresses. The 2D model is made for a local analysis allowing a more refined mesh; the stress distribution results obtained demonstrate a slight difference in their extreme values of the adhesive, attributed to boundary singularities of the model.

Figure 8a shows that applying a horizontal force (T), the Bigwood and Crocombe formulas do not calculate the normal stress, however, the FEA model shows the normal stress.

Regarding the points defined in Figure 3, it can be shown in Figure 10 that when the force V is applied at point A, there is a shear stress value of 1.031 MPa, while at the extreme point B the shear stress is 3.076 MPa, this difference in stress is due to the moment reaction generated at the boundary condition in the adherent 2.

In Figures 11 and 12, the behavior of the stresses through the laminate and its interfaces is shown. The stresses of the adhesive are like those presented in the first interface of the adherents 1 and 2, therefore the thickness of the interface and the adhesive of the joint must be considered.

In Figure 12 of the 2D model, high-stress values are presented in the corner of the external laminate of the adherent 1 due to the stress concentration in this corner.

A tubular hybrid joint (see Figure 6) can be optimized based on the number of layers of the tubular laminate, configuration of the tubular structure, and the limit pressure that the FRP panel and the hybrid tubular joint can support. In cases where it is required to increase the pressure p , the FRP panel laminate should be reviewed utilizing critical layer analysis, and as an option closer vertical pipes can be installed.

5. Conclusions

Initially, for the preliminary design, the macro-structural analysis should be carried out on the scantling of the panel structure, using a Classification Society guideline. Then, a microstructural analysis of the laminate sequence should be carried out using a “critical layer” analysis. Finally, the hybrid tubular joint is dimensioned as an additional reinforcement of the panel, according to the forces acting on the hybrid joint.

The number of laminate layers on the tubular reinforcements depends on the type of design load that are applied or transmitted to the panel and/or tubular hybrid joint; thus, the laminate scantling should be validated by the failure criteria using the interlaminar stresses.

The model considerations are applicable for the interlaminar study but do not include the calculation of the temperature or hygroscopic effects. Another aspect is the tubular laminate bevelling, as the maximum resulting stresses are located at the reinforced laminate ends. For this reason, we recommend that the bevel guide proposed by SSC-Lloyd’s Register be applied.

The proposed moment formula is recommended for tubular reinforcement. In the case where it is necessary to apply another structural reinforcement type, the formula must be modified, the compatibility and stresses between laminates should be analyzed.

The interlaminar stresses resulting from the outer layer are related to the possibility of debonding; however, in the case of sandwich panels as a second stage, we recommend analyzing the interlaminar and intralaminar stresses of all layers and the core. In no case, the core should be used perpendicular to the stress direction.

When comparing the interlaminar stress fraction recommended by SSC-Lloyd’s Register with that proposed by Hollaway, this fraction corresponds to 10^6 lifecycles, assuming that the core tie layer is CSM. Additionally, Hollaway proposed that the fraction may also have lower values than those recommended by SSC-Lloyd’s Register, depending on the fatigue applied. For this reason, we recommend researching the variation of the interlaminar stress fraction as a function of fatigue.

The formulas proposed for the shear and normal stress estimation showed satisfactory results when compared with the values obtained with FEA. The proposed methodology made possible the study of the behavior of the stresses obtained at the adhesive ends and the analysis of the resulting interlaminar stresses that are generated in the adherent’s adjacent outer layer. The stress analysis in of the remaining layers and the interlaminar effect on the core, is beyond the scope of this investigation, however, is an important topic of study in the future. For the proposed equations, the failure stresses for laminates of polyester resin with E fiberglass (FRP) are presented in Table 1.

The proposed methodology is aimed to facilitate the preliminary design of a tubular hybrid joint. The joint as designed allows to join the FRP panel with metal decks having the advantage of getting a watertight union, improving the contact area of the adhesive, and obtaining an inert hybrid metal structure, having as an additional advantage that, depending on the type of load condition on the FRP panel and steel deck, it is easy to increase the number of vertical reinforcements or the adhesive joint length.

Author Contributions: F.D.: introduction, summary, writing, methodology, tables, figures, validation of results, discussion. L.C.: work structure, discussion of results and conclusions. All authors have read and agreed to the published version of the manuscript.

Funding: This research received no external funding

Acknowledgments: The authors thank the ESPOL Polytechnic University, Escuela Superior Politécnica del Litoral, Faculty of Maritime Engineering and Marine Sciences (FIMCM), for the facilities provided with the laboratory.

Conflicts of Interest: The authors declare that they have no known competing for financial interests or personal relationships that could have appeared to have influenced the work reported in this paper.

Nomenclature

A_{ij}	Extensional stiffness matrix	S_t	Shear interlaminar stress limit
c	Half-length of adhesive	t	Adhesive thickness
C	Contiguity factor, Ueruma	T	x -direction force on tubular reinforcement laminate
D	Tubular reinforcement diameter	T_c	y -direction force on the adhesive joint, for Bigwood formulation
d_1	Distance from the neutral axis of adhesive to the applied load	V	z -direction force on tubular reinforcement laminate
D_1	Adherent 1 rigidity	V_f	Volume fraction of fibers of individual ply
D_2	Adherent 2 rigidity	V_m	Volume fraction of resin
E_a	Adhesive elasticity modulus	V_y	y direction components of force V on tubular reinforcement laminate
E_f	Elasticity modulus of the fibers	V_z	z direction components of force V on tubular reinforcement laminate
E_{ij}	Elasticity modulus of individual ply E_{i1} y E_{i2} , Equation (21a)	V_c	z -direction force on the adhesive joint, for Bigwood formulation
E_i^{i-p}	Elasticity modulus of individual ply: E_x, E_y and E_z , Table A1	x	Longitudinal direction
E_i	Elasticity modulus of adherent laminate: E_x, E_y and E_z , Table A2	y	Transverse direction
E_{mj}	Elasticity modulus of the resin E_{m1} y E_{m2} , Equation (21a)	z	Vertical direction
E_m	Elasticity modulus of the resin	Z_t	Normal interlaminar stress limit
E_1	Adherent 1 elasticity modulus, Table A3	α_1	Adherent compliance factor 1 for shear stress, Bigwood formulation
E_2	Adherent 2 elasticity modulus, Table A3	α_2	Adherent compliance factor 2, Bigwood formulation
f_c	Fiber content of individual ply	β_1	Adherent compliance factor 1 for normal stress, Bigwood formulation
F_{rc-i}	Interlaminar stress fraction	β_2	Adherent compliance factor 2 for normal stress, Bigwood formulation
G_a	Adhesive shear modulus	ξ_1	Exponent of the tension distribution of flexure in the adherent, Hart-Smith
G_i^{i-p}	Shear modulus of individual ply: G_x, G_y and G_z , Table A1	$\epsilon_i, \epsilon_{ij}$	Mid-surface strains

G_i	Shear modulus of adherent laminate: G_x, G_y and G_z , Table A2	ρ	Density kg/m^3
G_f	Shear modulus of the fibers	σ_{Tc}	Normal interlaminar stress due to axial force (T_c), Bigwood formulation
G_m	Shear modulus of the resin	σ_{Vc}	Normal interlaminar stress due to shear force (V_c), Bigwood formulation
h_k	Thickness of individual ply	σ_{Mc}	Normal interlaminar stress due to moment (M_c), Bigwood formulation
h_1	Adherent 1 thickness	σ_z	Total normal interlaminar stress
h_2	Adherent 2 thickness	μ_i^{i-p}	Poisson coefficient of individual ply: μ_x, μ_y and μ_z , Table A1
k_1	Eccentricity factor, Hart-Smith	μ_i	Poisson coefficient of adherent laminate: μ_x, μ_y , and μ_z , Table A2
k_b	Parameter of flexural stiffness for compound adherents, Hart-Smith	μ_f	Poisson coefficient for the fiber
K_5	Constant of tension differential equations of normal stress, Bigwood formulation	μ_m	Poisson coefficient for the resin
K_6	Constant of tension differential equations of shear stress, Bigwood formulation	μ_1	Adherent 1 Poisson coefficient
L	Length of adhesive, $L = 2 \cdot c$	μ_2	Adherent 2 Poisson coefficient
M_c	x-moment on the adhesive joint, Bigwood formulation	τ_{yz}	Total shear interlaminar stress on yz direction
M'	Equivalent moment on tubular reinforcement laminate	τ_{xz}	Total shear interlaminar stress on xz direction
M_{H-S}	Adhesive joint moment, Hart-Smith	τ_{Tc}	Shear interlaminar stress due to axial force (T_c)
\bar{Q}_{ij}	Lamination parameter, Appendix B.1.1	τ_{Vc}	Shear interlaminar stress due to shear force (V_c)
p	Design pressure kN/m^2	τ_{Mc}	Shear interlaminar stress due moment (M_c)
P	y-direction force on tubular reinforcement laminate	ζ_f	Specific gravity of fiber in individual ply
S_f	Safety factor	ζ_R	Specific gravity of resin in individual ply

Abbreviations

CSM	Chopped strand mat (fiberglass)
CFRP	Carbon fiber reinforced polymer
DNV	Det Norske Veritas
FEA	Finite element analysis
FRP	Fiber-reinforced plastic
NJC	US Navy ONR's Navy Joining Center
SSC	Special Service Craft
UD	Uni-directional fiber
WR	Woven Roving (Fiberglass)

Appendix A

Input Data, Properties of Fiber, Resin, and Core

Properties on (xy) plane of fibers, core, and resin are defined using Lloyd's Register [39] guidelines. Properties of transversal planes (yz and xz) are estimated with formulas of Appendix B.

Table A1. Fibers, resin, and core properties for individual ply.

Properties	Symbol	CSM 300	CSM 450	WR 800	Balsa	Polyester Resin
Density (kg/m ³)	ρ	1384	1428	1634	144	1200
Elasticity modulus <i>x</i> -direction (N/mm ²)	E_x^{i-p}	5750	6500	14,500	67.80	3400
Elasticity modulus <i>y</i> -direction (N/mm ²)	E_y^{i-p}	5750	6500	14,500	67.80	3400
Elasticity modulus <i>z</i> -direction (N/mm ²)	E_z^{i-p}	4169	4414	6017	3900	3400
Shear modulus <i>xy</i> -direction (N/mm ²)	G_{xy}^{i-p}	2665	2750	3090	19	1250
Shear modulus <i>xz</i> -direction (N/mm ²)	G_{xz}^{i-p}	1607	1713	2364	129	1250
Shear modulus <i>yz</i> -direction (N/mm ²)	G_{yz}^{i-p}	1607	1713	2364	129	1250
Poisson coefficient <i>xy</i>	μ_{xy}^{i-p}	0.340	0.340	0.320	0.285	0.360
Poisson coefficient <i>xz</i>	μ_{xz}^{i-p}	0.340	0.330	0.300	0.014	0.360
Poisson coefficient <i>yz</i>	μ_{yz}^{i-p}	0.340	0.330	0.300	0.014	0.360

Table A2 presents the orthotropic properties for the adherent’s laminates 1 and 2, calculated with the formulas indicated in Appendix B.1.1.

Table A2. Orthotropic properties of adherents.

Properties	Symbol	Adherent 1 ⁽¹⁾	Adherent 2 ⁽²⁾
Density (kg/m ³)	ρ	1513	499
Thickness (mm)	h	4.030	32.900
Elasticity modulus <i>x</i> -direction (N/mm ²)	E_x	8569	2064
Elasticity modulus <i>y</i> -direction (N/mm ²)	E_y	8569	2064
Elasticity modulus <i>z</i> -direction (N/mm ²)	E_z	5119	4249
Shear modulus <i>xy</i> -direction (N/mm ²)	G_{xy}	2713	652
Shear modulus <i>xz</i> -direction (N/mm ²)	G_{xz}	1770	166
Shear modulus <i>yz</i> -direction (N/mm ²)	G_{yz}	1770	166
Poisson coefficient <i>xy</i>	μ_{xy}	0.421	0.421
Poisson coefficient <i>xz</i>	μ_{xz}	0.490	0.170
Poisson coefficient <i>yz</i>	μ_{yz}	0.490	0.170
Poisson coefficient <i>yx</i>	μ_{yx}	0.421	0.421
Poisson coefficient <i>zx</i>	μ_{zx}	0.293	0.349
Poisson coefficient <i>zy</i>	μ_{zy}	0.293	0.349

Note: (1) Laminate 1: CSM450 + WR800 + CSM450 + CSM450. (2) Laminate 2: CSM300 + CSM450 + WR800 + CSM450 + Balsa 25mm + CSM450 + WR800 + CSM450 + CSM300.

Table A3 presents the equivalent isotropic properties resulting from the orthotropic laminate of adherents 1 and 2 (see Table A2), using the formulas indicated in Appendix B.1.3. This equivalence is necessary to apply the Bigwood and Crocombe [24] formulas indicated in Section 2.1.2 and Appendix C.

Table A3. Equivalent isotropic properties of adherents.

Properties	Symbol	Adherent 1	Adherent 2
Elasticity modulus (N/mm ²)	E	6171	2157
Shear modulus (N/mm ²)	G	2151	730
Poisson coefficient	μ	0.435	0.477

Appendix B

Appendix B.1. Formulas to Estimate Equivalent Properties

Appendix B.1.1. Stress–Strain Matrix

The presented formulas correspond to the stress–strain matrix according to the classical lamination theory.

$$[\sigma_{ij}] = \begin{bmatrix} \bar{Q}_{11} & \bar{Q}_{12} & \bar{Q}_{13} & 0 & 0 & 0 \\ \bar{Q}_{12} & \bar{Q}_{22} & \bar{Q}_{23} & 0 & 0 & 0 \\ \bar{Q}_{13} & \bar{Q}_{23} & \bar{Q}_{33} & 0 & 0 & 0 \\ 0 & 0 & 0 & \bar{Q}_{44} & 0 & 0 \\ 0 & 0 & 0 & 0 & \bar{Q}_{55} & 0 \\ 0 & 0 & 0 & 0 & 0 & \bar{Q}_{66} \end{bmatrix} \cdot \begin{bmatrix} \varepsilon_1 \\ \varepsilon_2 \\ \varepsilon_3 \\ 2 \cdot \varepsilon_{23} \\ 2 \cdot \varepsilon_{31} \\ 2 \cdot \varepsilon_{12} \end{bmatrix} \tag{A1}$$

$$A_{ij} = \sum_{k=1}^N (\bar{Q}_{ij})_k \cdot h_k, \quad i, j \leq 3 \text{ and } i, j = 6, \tag{A2}$$

$$A_{ij} = \sum_{k=1}^N \frac{h_k}{(\bar{Q}_{ij})_k}, \quad i, j = 4, 5. \tag{A3}$$

Parameters \bar{Q}_{ij} are defined on Vinson [38].

Properties of orthotropic laminates are defined by Naughton [40]: generalized formulas.

$$E_x = \frac{A_{11} \cdot A_{22} - A_{12}^2}{h \cdot A_{22}}, \quad E_y = \frac{A_{11} \cdot A_{22} - A_{12}^2}{h \cdot A_{11}}, \quad E_z = \frac{A_{11} \cdot A_{33} - A_{13}^2}{h \cdot A_{11}} \tag{A4}$$

$$G_{xy} = \frac{A_{66}}{h}, \quad G_{xz} = \frac{h}{A_{55}}^{(*)}, \quad G_{yz} = \frac{h}{A_{44}}^{(*)} \tag{A5}$$

$$\mu_{xy} = \frac{A_{12}}{A_{22}}, \quad \mu_{xz} = \frac{A_{13}}{A_{33}}, \quad \mu_{yz} = \frac{A_{23}}{A_{33}} \tag{A6}$$

(*) Modified as following [41]

Appendix B.1.2. Formulas to Estimate Properties of Fiber in the Transverse Direction

The formulas for estimating the modulus of elasticity z-direction, shear modulus, and Poisson’s coefficient in the xz and yz planes for an individual ply are proposed by Tsai [42]:

$$E_z^{i-p} = 2[1 - \mu_f + (\mu_f - \mu_m) \cdot V_m] \cdot \left[(1 - C) \frac{K_f \cdot (2K_m + G_m) - G_m \cdot (K_f - K_m) \cdot V_m}{(2K_m + G_m) + 2(K_f - K_m) \cdot V_m} + C \frac{K_f \cdot (2K_m + G_f) + G_f \cdot (K_m - K_f) \cdot V_m}{(2K_m + G_f) - 2(K_m - K_f) \cdot V_m} \right] \tag{A7}$$

$$G_{xz}^{i-p} = (1 - C) \cdot G_m \frac{2G_f - (G_f - G_m) \cdot V_m}{2G_m + (G_f - G_m) \cdot V_m} + C \cdot G_f \frac{(G_f + G_m) - (G_f - G_m) \cdot V_m}{(G_f + G_m) + (G_f - G_m) \cdot V_m}, \tag{A8}$$

$$\mu_{xz}^{i-p} = (1 - C) \frac{K_f \cdot \mu_f \cdot (2K_m + G_m) \cdot V_f + K_m \cdot \mu_m \cdot (2K_f + G_m) \cdot V_m}{K_f \cdot (2K_m + G_m) - G_m \cdot (K_f - K_m) \cdot V_m} + C \cdot \frac{K_m \cdot \mu_m \cdot (2K_f + G_f) \cdot V_m + K_f \cdot \mu_f \cdot (2K_m + G_f) \cdot V_f}{K_f \cdot (2K_m + G_f) + G_f \cdot (K_m - K_f) \cdot V_m}, \tag{A9}$$

Shear modulus and Poisson’s coefficient in the yz plane are equal to those of de xz plane.

where:

$$K_f = \frac{E_f}{2(1 - \mu_f)}, \quad K_m = \frac{E_m}{2(1 - \mu_m)}, \tag{A10a}$$

$$G_f = \frac{E_f}{2(1 + \mu_f)}, \quad G_m = \frac{E_m}{2(1 + \mu_m)}. \tag{A10b}$$

The contiguity factor C is defined by Ueruma [43], as:

$$C = 0.4V_f - 0.025. \tag{A11}$$

The volume fraction V_f of the fiber is determined from [39]:

$$V_f = \frac{f_c \cdot \zeta_R}{f_c \cdot \zeta_R - f_c \cdot \zeta_f + \zeta_f}. \tag{A12}$$

Appendix B.1.3. Formulas to Estimate Equivalent Isotropic Properties from Orthotropic Properties

Akasaka [44] proposes formulas to estimate equivalent isotropic properties based on the orthotropic properties defined by Equations (A4)–(A6).

$$E = \left[\frac{E_x + E_z + 2\mu_{xz} \cdot E_z}{1 - \mu_{xz} \cdot \mu_{zx}} \right] \cdot \left[\frac{E_x + E_z - 2\mu_{xz} \cdot E_z + 4(1 - \mu_{xz} \cdot \mu_{zx}) \cdot G_{xz}}{3(E_x + E_z) + 2 \cdot \mu_{xz} \cdot E_z + 4(1 - \mu_{xz} \cdot \mu_{zx}) \cdot G_{xz}} \right], \tag{A13}$$

$$G = \frac{E_x + E_z - 2\mu_{xz} \cdot E_z}{8(1 - \mu_{xz} \cdot \mu_{zx})} + \frac{G_{xz}}{2}, \tag{A14}$$

$$\mu = \frac{E}{2G} - 1. \tag{A15}$$

Appendix C

General Elastic Analysis

Below the formulas to estimate the distribution of stresses proposed by Bigwood and Crocombe [24] are described:

Normal stress formula:

$$\sigma_z = A_1 \cdot \cos(K_5 \cdot y) \cdot \cosh(K_5 \cdot y) + A_2 \cdot \cos(K_5 \cdot y) \cdot \sinh(K_5 \cdot y) + A_3 \cdot \sin(K_5 \cdot y) \cdot \cosh(K_5 \cdot y) + A_4 \cdot \sin(K_5 \cdot y) \cdot \sinh(K_5 \cdot y), \tag{A16}$$

where:

$$D_1 = \frac{E_1 \cdot h_1^3}{12 \cdot (1 - \mu_1^2)}, \quad D_2 = \frac{E_2 \cdot h_2^3}{12 \cdot (1 - \mu_2^2)}, \tag{A17}$$

$$K_5^4 = \frac{E_a}{4 \cdot t} \left(\frac{1}{D_1} + \frac{1}{D_2} \right), \tag{A18}$$

$$A_1 = \frac{b_3 \cdot R_3 - 2 \cdot b_2 \cdot \sinh(K_5 \cdot L) \cdot \sin(K_5 \cdot L) + b_1 \cdot R_6 + b_4 \cdot R_1}{R_5}, \tag{A19a}$$

$$A_2 = \frac{b_2 \cdot R_2 - b_3 \cdot \sinh^2(K_5 \cdot L) - b_1 \cdot R_4 - b_4 \cdot \sinh(K_5 \cdot L) \cdot \sin(K_5 \cdot L)}{R_5}, \tag{A19b}$$

$$A_3 = \frac{b_2 \cdot R_2 - b_3 \cdot \sin^2(K_5 \cdot L) - b_1 \cdot R_4 - b_4 \cdot \sinh(K_5 \cdot L) \cdot \sin(K_5 \cdot L)}{R_5}, \tag{A19c}$$

$$A_4 = b_1, \tag{A19d}$$

$$b_1 = \frac{E_a}{2 \cdot K_5^2 \cdot t} \left(\frac{M_{c21}}{D_2} - \frac{M_{c11}}{D_1} \right), \quad b_2 = \frac{E_a}{2 \cdot K_5^2 \cdot t} \left(\frac{M_{c22}}{D_2} - \frac{M_{c12}}{D_1} \right), \tag{A20a}$$

$$b_3 = \frac{E_a}{2 \cdot K_5^3 \cdot t} \left(\frac{V_{c21}}{D_2} - \frac{V_{c11}}{D_1} \right), \quad b_4 = \frac{E_a}{2 \cdot K_5^3 \cdot t} \left(\frac{V_{c22}}{D_2} - \frac{V_{c12}}{D_1} \right), \tag{A20b}$$

$$R_1 = \cosh(K_5 \cdot L) \cdot \sin(K_5 \cdot L) - \sinh(K_5 \cdot L) \cdot \cos(K_5 \cdot L), \tag{A21a}$$

$$R_2 = \cosh(K_5 \cdot L) \cdot \sin(K_5 \cdot L) + \sinh(K_5 \cdot L) \cdot \cos(K_5 \cdot L), \tag{A21b}$$

$$R_3 = \cosh(K_5 \cdot L) \cdot \sinh(K_5 \cdot L) - \cos(K_5 \cdot L) \cdot \sin(K_5 \cdot L), \tag{A21c}$$

$$R_4 = \cosh(K_5 \cdot L) \cdot \sinh(K_5 \cdot L) + \cos(K_5 \cdot L) \cdot \sin(K_5 \cdot L), \tag{A21d}$$

$$R_5 = \sinh^2(K_5 \cdot L) - \sin^2(K_5 \cdot L), \tag{A21e}$$

$$R_6 = \cosh^2(K_5 \cdot L) - \cos^2(K_5 \cdot L). \tag{A21f}$$

Shear stress formula:

$$\tau_{yz} = B_1 \cdot \cosh(K_6 \cdot y) + B_2 \cdot \sinh(K_6 \cdot y) + B_3, \quad (\text{A22})$$

where:

$$K_6^2 = \frac{4 \cdot G_a}{t} \left(\frac{1 - \mu_1^2}{E_1 \cdot h_1} + \frac{1 - \mu_2^2}{E_2 \cdot h_2} \right), \quad (\text{A23})$$

$$B_1 = \frac{c_2 - c_1 \cdot \cosh(K_6 \cdot L)}{K_6 \cdot \sinh(K_6 \cdot L)}, \quad B_2 = \frac{c_1}{K_6}, \quad B_3 = \frac{c_3}{L} - \frac{c_2 - c_1}{K_6^2 \cdot L}, \quad (\text{A24})$$

$$c_1 = \frac{G_a}{t} \left[\frac{1 - \mu_1^2}{E_1 \cdot h_1} \left(T_{c11} - \frac{6 \cdot M_{c11}}{h_1} \right) - \frac{1 - \mu_2^2}{E_2 \cdot h_2} \left(T_{c21} + \frac{6 \cdot M_{c21}}{h_2} \right) \right], (**), \quad (\text{A25a})$$

$$c_2 = \frac{G_a}{t} \left[\frac{1 - \mu_1^2}{E_1 \cdot h_1} \left(T_{c12} - \frac{6 \cdot M_{c12}}{h_1} \right) - \frac{1 - \mu_2^2}{E_2 \cdot h_2} \left(T_{c22} + \frac{6 \cdot M_{c22}}{h_2} \right) \right], (**), \quad (\text{A25b})$$

$$c_3 = (T_{c12} - T_{c11}) \left(1 - \frac{y}{L} \right) + (T_{c21} - T_{c22}) \left(\frac{y}{L} \right), (**), \quad (\text{A25c})$$

(D_1, h_1, μ_1, E_1) and (D_2, h_2, μ_2, E_2) correspond to adherent 1 and adherent 2, respectively.

$T_{c11}, V_{c11}, M_{c11}, T_{c12}, V_{c12}, M_{c12}$, are the forces applied to the extremes of adherent 1.

$T_{c22}, V_{c22}, M_{c22}, T_{c21}, V_{c21}, M_{c21}$, are the forces applied to the extremes of adherent 2.

(**) For a better understanding, the nomenclature of the original variables b_1, b_2 , and b_3 of the shear stress formula in [24], are changed to c_1, c_2 , and c_3 .

References

- Ritter, G.; Speth, D.; Yang, Y. Qualifications of Adhesives for Marine Composite-to-Steel Bonded Applications. *J. Ship Prod.* **2009**, *25*, 198–205.
- Rudiger, J.; McGeorge, D. Science and Technology of Bolt-Adhesive Joints. *Adv. Struct. Mater.* **2011**, *6*, 177–199.
- Hentinen, M.; Hildebrand, M. How to efficiently join FRP structures to metal ships? In Proceedings of the 3rd International Conference on Fast Sea Transportation, FAST'95, Lübeck-Travemünde, Germany, 25–27 September 1995.
- Hentinen, M.; Hildebrand, M.; Visuri, M. *Adhesively Bonded Joints between FRP Sandwich and Metal—Different Concepts and Their Strength Behaviour*; Research Notes 1862; VTT Manufacturing Tech., Centre of Finland, VTT Tiedotteita, Meddelanden: Espoo, Finland, 1997; 44p, ISBN 951-38-5183-4.
- Bohlmann, R.E.; Fogarty, J.H. Demonstration of a composite to steel deck joint on a Navy destroyer. In Proceedings of the 9th International Conference on Marine Applications of Composite Materials, Melbourne, FL, USA, 19–21 March 2002.
- Kotsidis, E.; Kouloukouras, I.; Tsouvalis, N. Finite element parametric study of a composite to steel join. In Proceedings of the 2nd International Conference on Maritime Technology and Engineering, Lisbon, Portugal, 15–17 October 2014.
- Shkolnikov, V. *Hybrid Ship Hulls, Engineering Design Rationales*; Butterworth-Heinemann: New York, NY, USA, 2014.
- Simler, J.; Brown, L. 21st Century Surface combatants require improved composite to Steel adhesive bonds. *AMPTIAC Q.* **2003**, *7*, 21–27.
- Boyd, S.; Blake, J.; Shenoi, R.; Kapadia, A. Integrity of hybrid steel to composite joints for marine application. *Eng. Marit. Environ.* **2014**, *218*, 235–246. [[CrossRef](#)]
- Ozes, C.; Neser, N. *Experimental Study on Steel to FRP Bonded Lap Joints in Marine Applications*; Dokuz Eylul University, Hindawi Publishing Corporation: Konak, Turkey, 2015.
- Babazadeh, A.; Reza, M. Finite Element Investigation of Performance of Composite-Steel Double Lap Adhesive Joint Under Tensile Loading. *Lat. Am. J. Solids Struct.* **2017**, *14*, 277–291. [[CrossRef](#)]
- Johansson, H. Superstructure in FRP Composites, Saab, 01-41020236-000/Issue 00. 2016. Available online: <http://e-lass.eu/media/2016/08/Superstructures-in-FRP-composites-Henrik-Johansson.pdf> (accessed on 16 April 2020).

13. Beeston, A. Developments in fire protection of FRP composite vessels. In Proceedings of the RINA, Innovation in High-Speed Marine Vessels, Freemantle, Australia, 28–29 January 2009; Available online: <https://e-lass.eu/media/2016/08/RINA-Conference-Paper.pdf> (accessed on 16 April 2020).
14. Dominguez, J.; Carral, L. Hybrid Joint Between Steel Deck and Fiberglass Superstructure. In Proceedings of the Multidisciplinary International Conference of Research Applied to Defense and Security MICRADS, Salinas, Ecuador, 18–20 April 2018; Howlett, R.J., Ed.; Springer: Cham, Switzerland, 2018; Volume 94, pp. 284–295. [[CrossRef](#)]
15. Dominguez, J.; Carral, L. Superstructure Design: Combination of Fiberglass Panel and Tubular Structure with Naval Steel Hull. In Proceedings of the 25th Pan-American Conference of Naval Engineering—COPINAVAL, Panama City, Panama, 16–19 October 2017; Sáenz, A.V., Pereira, N.N., Couce, L.M.V., Formoso, J.A.F., Eds.; Springer: Cham, Switzerland, 2018; pp. 81–91. [[CrossRef](#)]
16. Volkersen, O. Die Nietkraftverteilung in Zugbeanspruchten Nietverbindungen Mit Konstanten Laschenquerschnitten (The rivet load distribution in lap-joints with members of constant thickness subjected to tension). *Luftfahrtforschung* **1938**, *15*, 41–47.
17. Goland, M.; Reissner, E. The stresses in cemented joints. *Jpn. Appl. Mech.* **1944**, *11*, A17–A27.
18. Hart-Smith, L. *Adhesive Bonded Single Lap Joints*; Technical Report NASA CR-112236; National Aeronautics and Space Administration: Hampton, VA, USA, 1973.
19. Hart-Smith, L. *Adhesive Bonded Double Lap Joints*; Technical Report NASA CR-112235; National Aeronautics and Space Administration: Hampton, VA, USA, 1973.
20. Hart-Smith, L. *Non-Classical Adhesive Joints in Practical Aerospace Construction*; Technical Report NASA CR-112238; National Aeronautics and Space Administration: Hampton, VA, USA, 1973.
21. Hart-Smith, L. Further Developments in the Design and Analysis of Adhesive-Bonded Structural Joints. In *STP749-EB Joining of Composite Materials*; Kedward, K., Ed.; ASTM International: West Conshohocken, PA, USA, 1981; pp. 3–31. [[CrossRef](#)]
22. Hart-Smith, L. *Design Methodology for Bonded-Bolted Composite Joints*; Vol I: Analysis Derivations and Illustrative Solutions; Report AFWAL-TR-81-3154; Flight Dynamics Laboratory, AF Wright Aeronautical Laboratories, Wright - Patterson AFB: Montgomery County, OH, USA, 1982.
23. Allman, D. A theory for elastic stresses in adhesive-bonded lap joints. *Q. J. Mech. Appl. Math.* **1977**, *30*, 415–436. [[CrossRef](#)]
24. Bigwood, D.; Crocombe, A. Elastic Analysis and Engineering Design Formulae for Bonded Joints. *Int. J. Adhes. Adhes.* **1989**, *9*, 229–242. [[CrossRef](#)]
25. Bigwood, D.; Crocombe, A. Non-Linear Adhesive-Bonded Joint Design Analyses. *Int. J. Adhes. Adhes.* **1990**, *10*, 31–41. [[CrossRef](#)]
26. Oplinger, D. *A Layered Beam Theory for Single-Lap Joints*; Report MTL TR 91–23; US Laboratory Command: Adelphi, MA, USA, 1991; p. 44.
27. Zou, G.; Shahin, K.; Taheri, F. An analytical solution for the analysis of symmetric composite adhesively bonded joints. *Compos. Struct.* **2004**, *65*, 99–510. [[CrossRef](#)]
28. Renton, W.; Vinson, J. The Analysis and Design of Composite Material Bonded Joints Under Static and Fatigue Loadings, Department of Mechanical and Aerospace Engineering, University of Delaware, Air Force Office of Scientific Research. August 1973. Available online: <https://apps.dtic.mil/dtic/tr/fulltext/u2/766932.pdf> (accessed on 20 April 2020).
29. Ojalvo, I.; Eidinoff, H. Bond Thickness Effects Upon Stresses in Single-lap Adhesive Joints. *AIAA J.* **1978**, *16*, 204–211. [[CrossRef](#)]
30. Adams, R.; Mallick, V. A method for the stress analysis of lap joints, Taylor & Francis. *J. Adhes.* **1992**, *38*, 199–217. [[CrossRef](#)]
31. Smeltzer, S.; Klang, E. Analysis Method for Inelastic, Adhesively Bonded Joints with Anisotropic Adherends, NASA Technical Reports Server, Proceedings of the American Society for Composites 18th Technical Conference, Paper Number 104. January 2003. Available online: <https://ntrs.nasa.gov/search.jsp?R=20040034208> (accessed on 20 April 2020).
32. Echtermeyer, A.; Ekeberg, T.; Sund, O. *Long-Term Testing of Composite Through-Thickness Properties*; Det Norske Veritas, Research Report 131; Novik: Nordland, Norway, 2004.
33. Hollaway, L. *Handbook of Polymer Composites for Engineers*; British Plastic Federation: Cambridge, UK, 1994.

34. Huang, J.; Garnier, C.; Pastor, M.; Gong, X. Rapid evaluation of S-N curve for composite laminates on thermographic approach. *MATEC Web Conf.* **2018**, *165*, 1–6. [[CrossRef](#)]
35. Nhamoinesu, S.; Overend, M. The Mechanical Performance of Adhesives for a Steel-Glass Composite Façade System. Proceedings of Challenging Glass 3-Conference on Architectural and Structural Applications of Glass, TU Delft, IOS Press BV, Amsterdam, The Netherlands, 28–29 June 2012; Volume 3, pp. 293–306. [[CrossRef](#)]
36. Riccio, A.; Sellitto, A. Analytical tool for the preliminary design of an adhesively bonded T joint. *Key Eng. Mater.* **2015**, *665*, 285–288. [[CrossRef](#)]
37. Hou, J.; Petrinic, N.; Ruiz, C. A Delamination Criterion for Laminated Composites under the Low-Velocity Impact. *Compos. Sci. Technol.* **2001**, *61*, 2069–2074. [[CrossRef](#)]
38. Vinson, J. *Plate and Panel Structures of Isotropic, Composite and Piezoelectric Materials, Including Sandwich Construction*; Solid Mechanics and Its Applications; Springer: Dordrecht, The Netherlands, 2005; pp. 1–423. ISBN 1-4020-3111-4.
39. Lloyds Register. Pat 8: Hull Construction in Composite. In *Rules and Regulations for the Classification of Special Service Craft*; Lloyd’s Register Group Limited: London, UK, 2019; pp. 586–722.
40. Naughton, B.; Panhuizen, F.; Vermeulen, A. The elastic properties of chopped strand mat and woven roving in G.R. laminae, Akzo Research, CO. Research Department. *J. Reinf. Plast. Compos.* **1985**, *4*, 195–204. [[CrossRef](#)]
41. Jones, R. Mechanics of composite materials. In *Taylor & Francis*, 2nd ed.; CRC Press: Philadelphia, PA, USA, 1999. [[CrossRef](#)]
42. Tsai, S. *Structural Behaviour of Composite Materials, National Aeronautics and Space Administration*; NASA CR-71: Washington, DC, USA, 1964.
43. Uemura, M.; Yamada, N. Elastic Constants of Carbon Fiber Reinforced Plastic Materials. *J. Soc. Mater. Sci.* **1975**, *24*, 156–163. [[CrossRef](#)]
44. Akasaka, T. A practical method of evaluating the isotropic elastic constants of glass mat reinforced plastics. *Compos. Mater. Struct. Jpn.* **1974**, *3*, 21.



© 2020 by the authors. Licensee MDPI, Basel, Switzerland. This article is an open access article distributed under the terms and conditions of the Creative Commons Attribution (CC BY) license (<http://creativecommons.org/licenses/by/4.0/>).